Molecular dynamics study of a dipolar fluid between charged plates

Song Hi Lee and Jayendran C. Rasaiah[a)]
Department of Chemistry, University of Maine, Orono, Maine 04469

J. B. Hubbard
Thermophysics Division, National Bureau of Standards, Gaithersburg, Maryland 20899

(Received 10 April 1986; accepted 25 July 1986)

Recent experiments and computer simulations of thin films have observed the segregation of nonpolar molecules into layers or sheets parallel to the confining walls. We discuss a molecular dynamics study of a thin film of Stockmayer molecules between Lennard-Jones plates and find that, in the absence of an electric field, the dipoles are mainly oriented parallel to the plates in each layer. The component of the dipole autocorrelation function in this plane decays to zero more slowly than the component perpendicular to the walls. The polarization density profile, with an electric field perpendicular to the plates, is also studied, and is found to oscillate from layer to layer, with a magnitude that is in excess of what is predicted by the Debye theory of dielectric saturation by a factor nearly equal to the ratio of the local density to the average bulk density.

I. INTRODUCTION

In an elegant experiment Horn and Israelachvili[1] measured the force between two molecularly smooth surfaces separated by a thin film of organic liquid and found it to exhibit spatial oscillations with a periodicity equal to the molecular size. Computer simulations of Lennard-Jones particles between two walls by Snook and van Megan[2] and by Magda *et al.*[3] have confirmed the presence of these oscillations and traced them to the formation of layers of molecules parallel to the walls. The distance between these layers is equal to the diameter of the molecules, confirming the importance of the repulsive forces between the particles in the fluid and between the particles and walls in inducing layering in a thin film trapped between two flat plates. The molecular dynamics simulations of Magda *et al.*[3] have also shown that the diffusive motion perpendicular to the walls is more strongly affected by confinement than the motion parallel to these surfaces. More recently, high density films of water between walls have been studied by computer simulation.[4,5] Lee *et al.*[4(a)] used the ST2 potential[4(b)] for water in their molecular dynamics study of a film of thickness 20 Å at 290 K between two model "hydrophobic" walls, and found density oscillations extending far into the fluid, with the molecules near the surface avoiding orientations that could lead to surface polarization. Christou *et al.*[5(a)] studied a film of thickness 23 Å between hard walls at 298 and 363 K by Monte Carlo simulation using the Rowlinson potential [5(b)] for the interaction between water molecules. The central section of the film, where the majority of molecules reside, was found to be more nearly like the bulk properties of water according to this model, leaving a rarefied region close to the walls and an oscillating density profile between the center and the edges of the film.

Several theoretical treatments predicting oscillations in the density and polarization density profiles of simpler model systems have appeared[6–10] over the past few years and it has been claimed[10] that, in the absence of an electric field, orientations parallel to the wall are favored by the molecules close to it. Our MD simulations for thin films confirm this prediction for a Stockmayer fluid and provide new information on the dynamics of dipoles in each layer of the film confined between two walls. A detailed study of the polarization density profiles in the presence of an electric field is also made.

II. SIMULATION OF THE STOCKMAYER FLUID BETWEEN TWO WALLS

The potential for the Stockmayer fluid[11] is given by

$$u_{ij}(\mathbf{r},\boldsymbol{\mu}_i,\boldsymbol{\mu}_j) = \underbrace{4\epsilon[(\sigma/r)^{12} - (\sigma/r)^6]}_{\text{LJ potential}} - \underbrace{\boldsymbol{\mu}_i \cdot \mathsf{T} \cdot \boldsymbol{\mu}_j}_{\text{DD potential}}, \tag{2.1}$$

where $\mathbf{r}$ is the vector joining particles i and j, $\boldsymbol{\mu}_i$ is the dipole moment vector of particle i, $r = |\mathbf{r}|$, and ϵ and σ are the Lennard-Jones parameters. The dipole interaction tensor

$$\mathsf{T} = (3\mathbf{rr}/r^2 - \mathsf{U})/r^3, \tag{2.2}$$

where U is the unit matrix. We use the method of constraints introduced by Ryckaert *et al.*[12] and adapted by Pollock and Alder[13] to Stockmayer fluids to treat the rotational part of the motion. The Lagrangian for particles of mass m and moment of inertia I with dipole moments μ interacting according the Stockmayer potential is

$$L = \sum_i \frac{1}{2} m v_i^2 + (1/\mu^2) \sum_i \frac{1}{2} I \dot{\boldsymbol{\mu}}_i^2 + \frac{1}{2} \sum_{i \neq j} \sum_j \boldsymbol{\mu}_i \cdot \mathsf{T} \cdot \boldsymbol{\mu}_j - \frac{1}{2} \sum_{i \neq j} \sum_j u_{ij}^{\mathrm{LJ}} + \sum_i \lambda_i (\mu_i^2 - \mu^2) + \sum_i \boldsymbol{\mu}_i \cdot \mathbf{E}. \tag{2.3}$$

The first two terms are the translational and rotational kinetic energies, respectively, and the third and fourth terms represent the dipole–dipole and Lennard-Jones interaction energies. The fifth term enables the components of $\boldsymbol{\mu}$ to be treated as independent variables in Cartesian rather than spherical polar coordinates, and thus a constraint term must be introduced with Lagrange multipliers determined such that $\mu^2 = |\boldsymbol{\mu}_i|^2$ at all times.[13] The last term in the Lagrangian

[a)] Present address: Department of Chemistry, University of Texas at Austin, Austin, TX 78712.

 0021-9606/86/215232-06$02.10

allows for the presence of an external field. The dipole–dipole potential energy, force, and torque on particle i may be written as

$$U_{DD,i} = [(\boldsymbol{\mu}_i \cdot \boldsymbol{\mu}_j)/r^3 - 3(\mathbf{r} \cdot \boldsymbol{\mu}_i)(\mathbf{r} \cdot \boldsymbol{\mu}_j)/r^5], \tag{2.4a}$$

$$\mathbf{F}_{DD,i} = -\nabla_{r_i} U_{DD,i} = \sum_{j \neq i} [\boldsymbol{\mu}_i \cdot \nabla_{r_i} \mathsf{T} \cdot \boldsymbol{\mu}_j]$$

$$= \sum_{j \neq i} \{3[\mathbf{r}(\boldsymbol{\mu}_i \cdot \boldsymbol{\mu}_j) + \boldsymbol{\mu}_i(\mathbf{r} \cdot \boldsymbol{\mu}_j) + \boldsymbol{\mu}_j(\mathbf{r} \cdot \boldsymbol{\mu}_i)]/r^5 - 15\mathbf{r}(\mathbf{r} \cdot \boldsymbol{\mu}_i)(\mathbf{r} \cdot \boldsymbol{\mu}_j)/r^7\}, \tag{2.4b}$$

$$\mathbf{T}_{DD,i} = -\nabla_{\mu_i} U_{DD,i} = \sum_{j \neq i} [\mathsf{T} \cdot \boldsymbol{\mu}_j]$$

$$= \sum_{j \neq i} [3\mathbf{r}(\mathbf{r} \cdot \boldsymbol{\mu}_j)/r^5 - \boldsymbol{\mu}_j/r^3]. \tag{2.4c}$$

Following earlier workers,[2,3] we consider the interaction between the fluid particles and a Lennard-Jones-type FCC solid, with the (100) planes parallel to the liquid–solid interface, by putting two flat semi-infinite solids at points $+\sigma$ and $-\sigma$ distant from the x–y planes of the rectangular box on the z axis. If the solid atoms are treated as being uniformly distributed across each plane, then the potential between the uppermost plane and a particle at a distance z away is obtained by integrating over the infinite LJ wall[14,15]

$$u_w(z) = 2\pi\epsilon[0.4(\sigma/z)^{10} - (\sigma/z)^4]. \tag{2.5}$$

The interaction of the entire infinite series of structureless planes with a given particle is described[2,3] by

$$u_w(z) = 2\pi\epsilon[0.4(\sigma/z)^{10} - (\sigma/z)^4 - (\sqrt{2}/3)(z/\sigma + 0.61/\sqrt{2})^{-3}] \tag{2.6}$$

and the particle-wall force is derived:

$$\mathbf{F}_w(z) = 8\pi\epsilon\mathbf{z}[(\sigma/z)^{10} - (\sigma/z)^4 - (\sqrt{2}z/4\sigma)(z/\sigma + 0.61/\sqrt{2})^{-4}]/z^2. \tag{2.7}$$

Since there are two such walls, the LJ wall–dipole interaction for particle i is given by

$$U_{w,i}(z_i) = u_w(z_i - z_1) + u_w(z_i - z_2), \tag{2.8a}$$

$$\mathbf{F}_{w,i}(z_i) = \mathbf{F}_w(z_i - z_1) + \mathbf{F}_w(z_i - z_2), \tag{2.8b}$$

where z_1 and z_2 are the locations of two walls.

The equation of motion for the translational degrees of freedom, derived from Eq. (2.3), is

$$m\ddot{\mathbf{r}}_i = \boldsymbol{\mu}_i \cdot \sum_{j \neq i} \nabla\mathsf{T} \cdot \boldsymbol{\mu}_j + \boldsymbol{\mu}_i \cdot \nabla\mathbf{E} + \mathbf{F}_i^{LJ}, \tag{2.9}$$

in which the last term represents the short range LJ force. For the rotational degrees of freedom, the equation of motion

$$(I/\mu^2)\ddot{\boldsymbol{\mu}}_i = \sum_{j \neq i} \mathsf{T} \cdot \boldsymbol{\mu}_j + \mathbf{E} + 2\lambda_i \boldsymbol{\mu}_i \tag{2.10}$$

also obtained from Eq. (2.3), involves the constraint λ_i. These equations are integrated using the *leapfrog* algorithm.[16] The equation for $\boldsymbol{\mu}_i^{n+1}$ at time step $(n+1)\,\Delta t$ involves solving a quadratic equation for λ_i found by demanding $\mu^2 = |\boldsymbol{\mu}_i^{n+1}|^2$ which leads to

$$\lambda_i = \frac{-c_1 + (c_1^2 - c_2 c_3)^{1/2}}{c_2}, \tag{2.11}$$

in which

$$c_1 = (2\mu^2/I)[\mu^2 + \boldsymbol{\mu}_i^n \cdot \dot{\boldsymbol{\mu}}_i^{n-1/2} + \mu^2(\boldsymbol{\mu}_i^n \cdot \mathbf{R}_i^n)/I], \tag{2.12}$$

$$c_2 = (2\mu^2/I)^2\mu^2, \tag{2.13}$$

$$c_3 = |\dot{\boldsymbol{\mu}}_i^{n-1/2}|^2 + (\mu^2/I)^2|\mathbf{R}_i^n|^2 + 2\boldsymbol{\mu}_i^n \cdot \dot{\boldsymbol{\mu}}_i^{n-1/2} + (2\mu^2/I)(\boldsymbol{\mu}_i^n \cdot \mathbf{R}_i^n + \dot{\boldsymbol{\mu}}_i^{n-1/2} \cdot \mathbf{R}_i^n), \tag{2.14}$$

where $\mathbf{R}_i^n$ is the sum of the first two terms on the right-hand side of Eq. (2.10) and $\boldsymbol{\mu}_i^n$ the dipole moment vector of the ith species in the nth step and $\dot{\boldsymbol{\mu}}_i^{n-1/2}$ is the time derivative of this vector halfway between the n-1th step and the nth step.

The simulation was carried out in a rectangular box of dimensions $7\times7\times h\sigma^2$ where h is the distance between the walls, set equal to 7.5σ, for the calculations reported here. The number of particles $N = 206$, the mass m of each particle was 6.63×10^{-26} g and the reduced temperature T^* $(= kT/\epsilon)$ and reduced density $\rho^* = \rho\sigma^3$ were 1.18 and 0.5605, respectively. The moment of inertia was assumed to be 0.025 m σ^2 and the time step Δt of 5 fs was used for the rotational and translational motions. Periodic boundary conditions were applied in the x and y directions parallel to the walls using the minimum image convention. Also, to take account of the long-range dipole–dipole interaction in the system, we performed Ewald summations in the x–y plane.[17–19]

Computations were first carried out for LJ particles between two LJ walls by setting the dipole moments equal to zero and suppressing the rotational part of the algorithm. Averages were computed over intervals of 10 000 time steps,

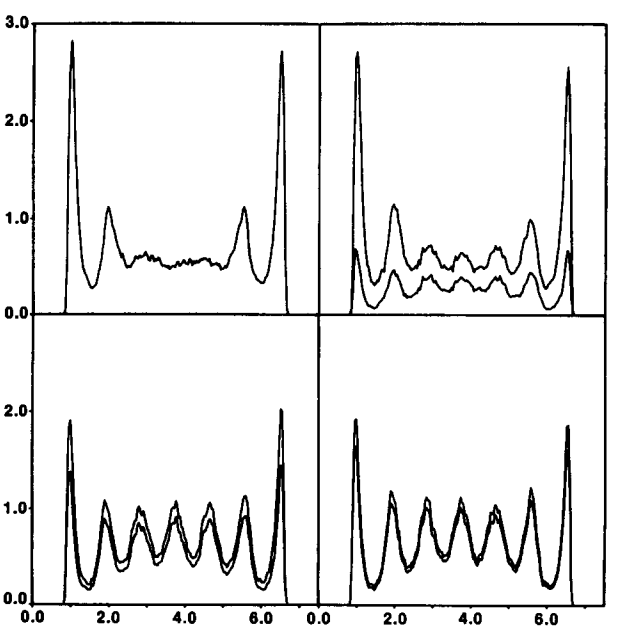

FIG. 1. The density and polarization density profiles for a Stockmayer fluid at an external field of $E = 0.0, 0.5, 1.5, 2.5\times10^9$ V m^{-1} perpendicular to the wall. The lower curves for nonzero fields are the polarization densities divided by the dipole moment $P_z(z,\mathbf{E})/\mu$. The reduced temperature $T^* = 1.18$.

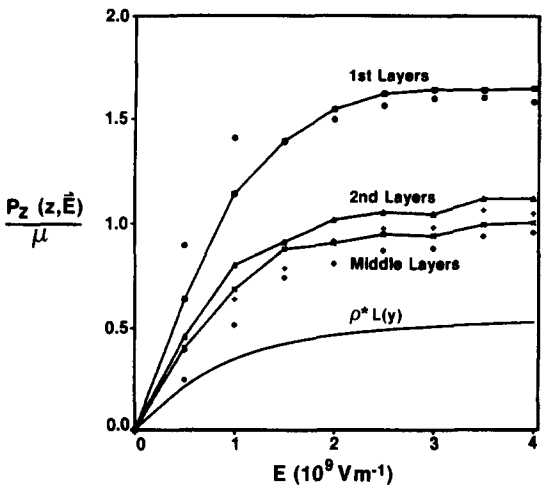

FIG. 2. The polarization densities $P_z(z,\mathbf{E})$ for different layers in the liquid film. The lowest curve is the average over the middle three peaks of Fig. 1. The circles, crosses, and diamonds are the corresponding results predicted by Eq. (3.3) using the density profiles $\rho(z)$ obtained from computer simulation.

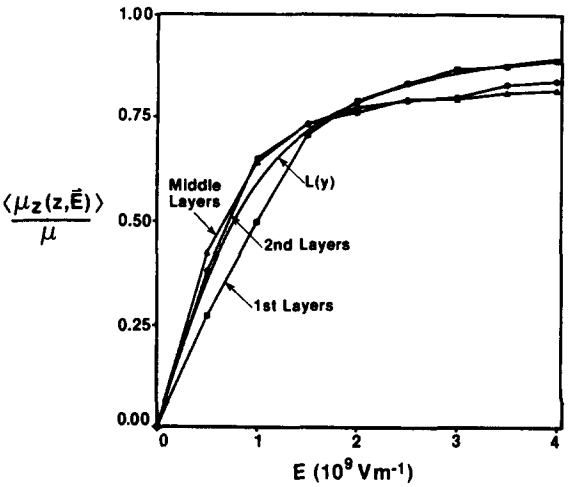

FIG. 3. The average of the component of the dipole moment in the z direction divided by the dipole moment $\langle\mu_z(z,\mathbf{E})\rangle/\mu$ for the different layers next to the wall as a function of the external field E. The smooth curve is the Langevin function which is the Debye equation for $\langle\mu_z(z,\mathbf{E})\rangle/\mu$.

after initial equilibration over 10 000 time steps, and the results found to be in excellent agreement with the Monte Carlo calculations of Snook and van Megan[2] and with the molecular dynamics simulations of Magda *et al.*[3] The point dipoles with a dipole moment $\mu = 1.36$ D were then embedded at random in the LJ particles in such a way that the total dipole moment and the total angular momentum of the system was zero. Again, after equilibration, averages were calculated over period of 10 000 time steps. We next added an electric field of the order of 10^9 V/m which corresponds to a surface charge density of one electronic charge /1000 Å^2. The interaction between the external electric field E and the dipole moment of each particle has no effect on the translational motion but modifies the rotational motion and orientation of the dipoles. Averages were computed after equilibration over intervals of 10 000 time steps. The density profiles were determined from a histogram of the z coordinates of the particles from one wall, i.e.,

$$\langle\rho(z,\mathbf{E})\rangle = \langle N_s(z,\Delta z;t)\rangle/A\Delta z, \tag{2.15}$$

where $N_s(z,\Delta z)$ is the number of particles whose centers lie in a slab of area A and thickness Δz with the midpoint of the slab at a distance z from the left wall and $\langle\cdots\rangle$ denotes the time average defined as the sum of $N_s(z,\Delta z)$ over successive time steps divided by their number. Likewise the polarization density is the time average of the dipole moment per unit volume in each slab which can be resolved into its components, for example,

TABLE I. Molecular dynamics results at the first and second peaks of the local density for a dipolar fluid between charged Lennard-Jones plates.

E (10^9 V m^{-1})		$\langle\rho(z)\rangle$	$\langle\mu_z(z)\rangle/\mu$	$\langle P_z(z)\rangle/\mu$	$\langle\rho(z)\rangle\langle\mu_z(z)\rangle/\mu$
0.0	First layers	2.6	0.0	0.0	0.0
	Second layers	1.1	0.0	0.0	0.0
0.5		2.5	0.27	0.64	0.68
		1.1	0.38	0.46	0.42
1.0		2.4	0.50	1.1	1.2
		1.1	0.65	0.80	0.72
1.5		2.0	0.70	1.4	1.4
		1.1	0.73	0.91	0.80
2.0		1.9	0.79	1.6	1.5
		1.2	0.77	1.0	0.92
2.5		1.9	0.83	1.6	1.6
		1.2	0.80	1.1	0.93
3.0		1.9	0.87	1.6	1.6
		1.2	0.80	1.0	0.96
3.5		1.8	0.87	1.6	1.6
		1.2	0.83	1.1	1.0
4.0		1.8	0.89	1.7	1.6
		1.2	0.84	1.1	1.0

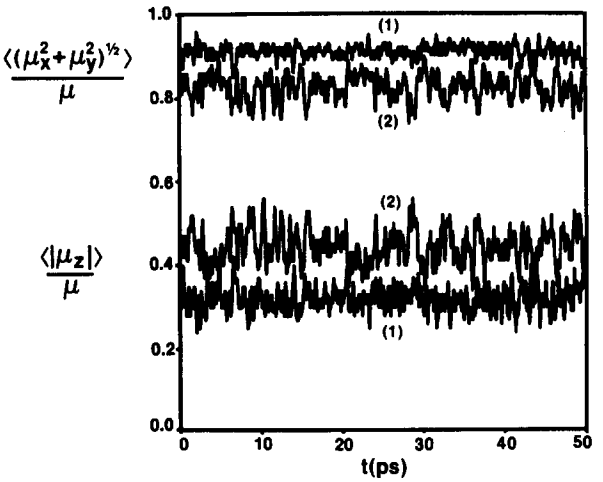

FIG. 4. The magnitudes of the components of the dipole moment parallel to and perpendicular to the wall as a function of time in the first two layers (labeled 1 and 2, respectively) as measured by $\langle(\mu_x^2+\mu_y^2)^{1/2}\rangle/\mu$ and $\langle|\mu_z|\rangle/\mu$.

$$\langle P_z(z,\mathbf{E})\rangle = \left\langle \sum_{i=1}^{N_s(t)} \mu_{z,i}(z,\Delta z;t) \right\rangle / A\Delta z, \tag{2.16}$$

where the sum is taken over the number of particles $N_s(z,\Delta z;t)$ at each time step in the slab. The components of the average dipole moment per particle in each slab are defined similarly, e.g.,

$$\langle \mu_z(z,\mathbf{E})\rangle = \left\langle \sum_{i=1}^{N_s(t)} \mu_{z,i}(z,\Delta z;t)/N_s(t) \right\rangle . \tag{2.17}$$

The width of the slits Δz used was 0.1σ. Averages of $|\mu_z|$ and of $(\mu_x^2+\mu_y^2)^{1/2}$ are also evaluated through analogous definitions. At high fields, when all the dipoles are aligned with the field (saturation) we naturally expect

$$\langle P_z(z,\mathbf{E})\rangle = \mu\langle \rho(z,\mathbf{E})\rangle. \tag{2.18}$$

III. RESULTS AND DISCUSSION

In Fig. 1 we have plotted the density and polarization density profiles for external electric fields E ranging from zero to 4.0×10^9 V m^{-1}. The density profile for the Stockmayer fluid in the absence of an electric field is essentially the same as that for the corresponding LJ system with some mild enhancement of the oscillations towards the center of the film and a slight decrease in the singlet density at the first peak near the wall. A marked change in these profiles occurs when the electric field is turned on, causing a further decrease in the local density near the wall and pronounced oscillations in this function across the film. Apparently the alignment of dipoles in the direction of the field increases the attractive interaction between them, causing them to retreat from the walls. As the field is increased the polarization density, which oscillates in phase with the local density, saturates to a limit given by Eq. (2.18). Figure 2 shows how the polarization density in each layer changes with the external field; the lowest simulation curve is the average over the middle three peaks. In Fig. 3 we have the corresponding curves for $\langle\mu_z(z,\mathbf{E})\rangle$ as a function of the external field E.

The Debye theory for ideal dipoles[20] in an electric field ignores the interaction between the dipoles and considers only their interaction with the external field, predicting

$$\langle\mu_z(z,\mathbf{E})\rangle = \mu L(y), \tag{3.1}$$

where $L(y)$ is the Langevin function and $y=(\mu|\mathbf{E}|)/kT$. There is of course no distinction between the different layers in this theory for $\langle\mu_z\rangle$; it was not constructed to handle thin films or the effects of the internal field created by the dipoles[21] in these films. Figure 3 shows that the theory predicts too small a value for $\langle\mu_z\rangle$ for all except the first layer at low fields. The overall agreement is however quite good. The polarization density profile is, by definition, the ensemble or time average,

$$\langle P_z(z,\mathbf{E})\rangle = \langle\rho(z,\mathbf{E})\mu_z(z,\mathbf{E})\rangle \tag{3.2}$$

and Eq. (2.18) follows from Eq. (3.2) at high fields (saturation). A theory at the level of simplicity introduced by Debye for $\langle\mu_z(z)\rangle$ can be constructed for $\langle P_z(z,\mathbf{E})\rangle$ by assuming that $\langle\rho(z)\mu_z(z,\mathbf{E})\rangle = \langle\rho(z)\rangle\langle\mu_z(z,\mathbf{E})\rangle$, from which it seems that

$$\langle P_z(z,\mathbf{E})\rangle = \langle\rho(z)\rangle\mu L(y) \tag{3.3}$$

if Eq. (3.1) is assumed for $\langle\mu_z(z,\mathbf{E})\rangle$. The first assumption is independent of the second and can be tested directly by simulation. Table I shows that its accuracy increases with

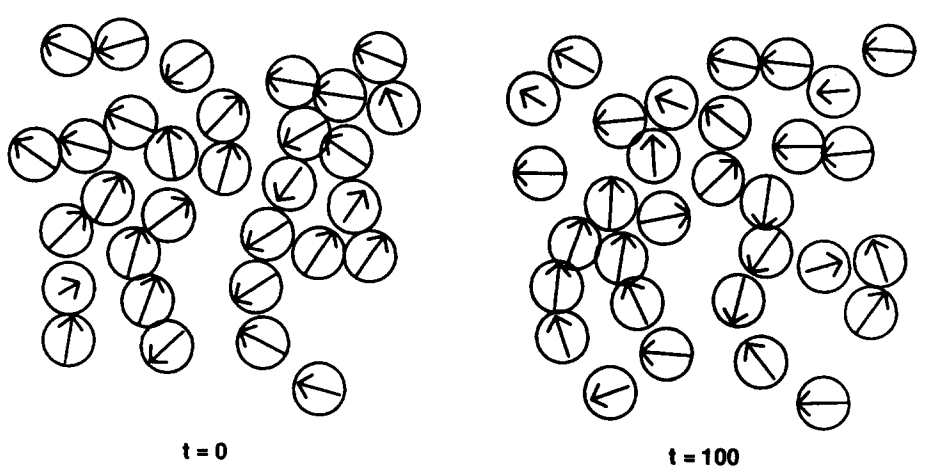

FIG. 5. Snapshots of the positions and orientations of dipoles in the first layer at intervals of 100 time steps. The length of the arrow in each circle is proportional to the component of the dipole moment parallel to the wall.

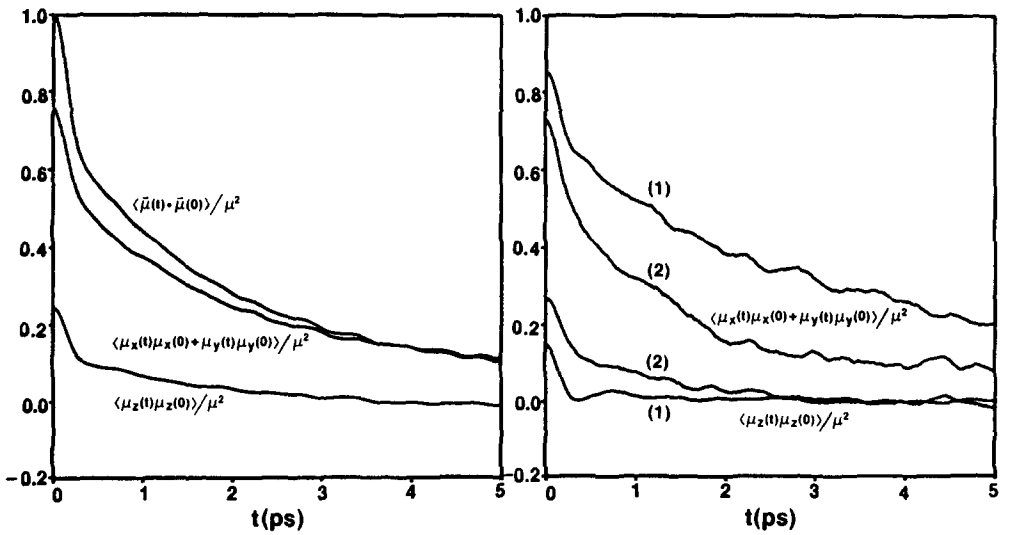

FIG. 6. (a) The dipole autocorrelation function $\langle \boldsymbol{\mu}(t) \cdot \boldsymbol{\mu}(0) \rangle / \mu^2$ and its transverse $\langle \mu_x(t)\mu_x(0) + \mu_y(t)\mu_y(0) \rangle / \mu^2$ and longitudinal $\langle \mu_z(t)\mu_z(0) \rangle / \mu^2$ components for all of the particles in the liquid film. (b) The averages of the transverse and longitudinal components of the dipole autocorrelation function for particles under the peaks nearest to (1) and next nearest to (2) the confining walls.

the field when the fluctuations in the number of particles in each layer are small. This could be used as the basis for a more elaborate theory of the polarization density profiles of thin films, particularly at high fields. Equation (3.3), which employs the additional assumptions implicit in the Debye theory[20,21] for $\langle \mu_z(z) \rangle$, distinguishes the polarization density profiles of the different layers as primarily due to variations in the corresponding density profiles. In Fig. 2 we compare this equation with our computer simulations and find that although it predicts saturation plausibly at high external fields, it gives polarization densities that are slightly large in the first layer, at low fields, and correspondingly small in the second and middle layers in order to conserve the total number of particles in the film. A different approximation which sets $\langle \rho(z) \rangle$ equal to the bulk or average density, is applicable only to the bulk fluid (i.e., $z \to \infty$).[21,22] Its usefulness is limited for thin films (see Fig. 2) since it ignores the oscillations in the local density that are characteristic of these films or of fluids close to a wall.[6–9] The polarization densities obtained from our simulations are greater than the predictions of this last approximation by a factor nearly equal to the ratio of the local density to the average bulk density (see Fig. 2).

We next consider the properties of the film in the absence of a field between the plates. An examination of the average values of $\langle (\mu_x^2 + \mu_y^2)^{1/2} \rangle / \mu$ and $\langle |\mu_z| \rangle / \mu$ shown in Fig. 4 for each of the first two peaks in the density profile immediately suggests that the dipoles are mainly oriented parallel to the wall with a probability that decreases slowly with the distance from the wall. In Fig. 5 snapshots of the particles in slits of width 0.3σ centered at the first peak near the left wall are shown at two different times separated by 100 time steps. The magnitude and length of the arrow drawn in each circle of radius $\sigma/2$ is proportional to the component of the dipole moment in the plane (x–y) parallel to the wall. These figures suggest that the dipoles in each layer have a tendency to form chains which correspond to configurations of low energy if the molecules are confined to layers and the net dipole moment of each layer is, on the average, zero. The rotational relaxation of the dipoles collectively and in each layer is of special interest. In Fig. 6(a) we plot the total orientation correlation function $\langle \boldsymbol{\mu}(t) \cdot \boldsymbol{\mu}(0) \rangle$ for all the particles as well as the components $\langle \mu_x(t)\mu_x(0) + \mu_y(t)\mu_y(0) \rangle$ and $\langle \mu_z(t)\mu_z(0) \rangle$ which are parallel and perpendicular to the walls, respectively. We find that the component of the correlation function parallel to the walls has a longer relaxation time than the component that is perpendicular to the walls. Figure 6(b) shows these same components for the particles under the peaks closest to the walls. Figure 7, which is again an average over all the particles, confirms that the time in which the transverse component of the dipole–dipole correlation function decays to zero is about 5000 time steps or 2.5×10^{-11} s whereas the longitudinal component vanishes after about 1000 time steps. Our simulations suggest that experiments to determine the relaxation times of dipoles in thin films between plates may be of great interest. Calculations of the solvation force and other

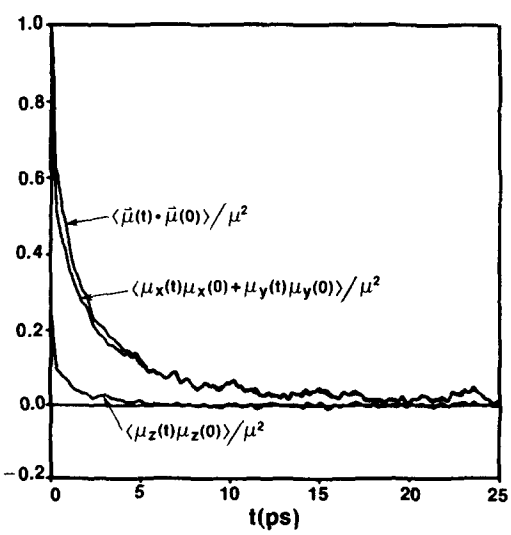

FIG. 7. The total dipole autocorrelation functions and its two components [see caption of Fig. 6(a)] over relatively long times (5000 time steps $= 2.5 \times 10^{-11}$ s).

properties as a function of the electric field for different plate separations will be reported in a forthcoming paper.

ACKNOWLEDGMENTS

This research was supported by the National Science Foundation under Grant No. CHE-8305747 to J. C. R. The computing and other facilities made available to S. H. L. and J. C. R. as guests at the National Bureau of Standards are most gratefully acknowledged.

[1]R. G. Horn and J. N. Israelachvili, Chem. Phys. Lett. **71**, 192 (1980).
[2]I. K. Snook and W. van Megan, J. Chem. Phys. **72**, 2907 (1980).
[3]J. J. Magda, M. Tirrell, and H. T. Davis, J. Chem. Phys. **83**, 1888 (1985).
[4](a) C. Y. Lee, J. A. McCammon, and P. J. Rossky, J. Chem. Phys. **80**, 4484 (1984); (b) F. H. Stillinger and A. Rahman, *ibid.* **60**, 1545 (1960).
[5](a) N. I. Christou, J. S. Whitehouse, D. Nicholson, and N. G. Parsonage, Mol. Phys. **55**, 397 (1985); (b) J. S. Rowlinson, Trans. Faraday Soc. **47**, 120 (1951).
[6]D. J. Isbister and B. C. Freasier, J. Stat. Phys. **20**, 331 (1979).
[7]J. Eggebrecht, D. J. Isbister, and J. C. Rasaiah, J. Chem. Phys. **73**, 3980 (1980).
[8]J. C. Rasaiah, D. J. Isbister, and J. Eggebrecht, J. Chem. Phys. **75**, 5497 (1981).
[9]M. J. Grimson and G. Rickayzen, Mol. Phys. **42**, 767, (1981).
[10]References to papers in press cited by J. P. Badiali, M. L. Rosinberg, and V. Russier, Mol. Phys. **56**, 105 (1985).
[11]W. H. Stockmayer, J. Chem. Phys. **9**, 398, 863, (1941).
[12]J. P. Ryckaert, G. Ciccotti, and H. J. C. Berendsen, J. Comp. Phys. **23**, 327 (1977).
[13]E. L. Pollock and B. J. Alder, Physica A **102**, 1 (1980).
[14]W. A. Steele, *The Interaction of Gases with Solid Surfaces* (Pergamon, Oxford, 1974).
[15]F. F. Abraham, J. Chem. Phys. **68**, 3713 (1978).
[16](a) R. W. Hockney, Methods Comput. Phys. **9**, 136 (1980); (b) D. Potter, *Computational Physics* (Wiley, London, 1972).
[17]D. J. Adams and I. R. McDonald, Mol. Phys. **32**, 931 (1976).
[18]V. W. Jansoone, Chem. Phys. **3**, 78 (1974).
[19]S. W. DeLeeuw, J. W. Perram, and E. R. Smith, Proc. R. Soc. London Ser. A **373**, 57 (1980), and references therein.
[20](a) P. Debye, Phys. Z. **13**, 97 (1912); (b) P. Debye, *Polar Molecules* (Dover, New York, 1928).
[21]L. Onsager J. Am. Chem. Soc. **58**, 1486 (1936).
[22]Improvements to the Debye theory of the polarization density at $z \rightarrow \infty$ have been discussed by Onsager (Ref. 21); J. C. Rasaiah, D. Isbister, and G. Stell, J. Chem. Phys. **75**, 4707 (1981); E. Martina and G. Stell, Phys. Rev. **24**, 2765 (1981).